Chemistry & Biology
Article

Small Molecule Activators of TRPML3

Christian Grimm,[1,5] Simone Jörs,[1,5] S. Adrian Saldanha,[2,5] Alexander G. Obukhov,[3] Bifeng Pan,[1] Kazuo Oshima,[1] Math P. Cuajungco,[4] Peter Chase,[2] Peter Hodder,[2] and Stefan Heller[1,*]
[1]Departments of Otolaryngology—Head and Neck Surgery, and Molecular and Cellular Physiology, Stanford University School of Medicine, Stanford, CA 94305, USA
[2]Scripps Research Institute Molecular Screening Center, The Scripps Research Institute, Scripps Florida, Jupiter, FL 33458, USA
[3]Department of Cellular and Integrative Physiology, Indiana University School of Medicine, IUPUI, Indianapolis, IN 46202, USA
[4]Department of Biological Science and Center for Applied Biotechnology Studies, California State University, Fullerton, CA 92831, USA
[5]These authors contributed equally to this work
*Correspondence: hellers@stanford.edu
DOI 10.1016/j.chembiol.2009.12.016

SUMMARY

We conducted a high-throughput screen for small molecule activators of the TRPML3 ion channel, which, when mutated, causes deafness and pigmentation defects. Cheminformatics analyses of the 53 identified and confirmed compounds revealed nine different chemical scaffolds and 20 singletons. We found that agonists strongly potentiated TRPML3 activation with low extracytosolic [Na^+]. This synergism revealed the existence of distinct and cooperative activation mechanisms and a wide dynamic range of TRPML3 activity. Testing compounds on TRPML3-expressing sensory hair cells revealed the absence of activator-responsive channels. Epidermal melanocytes showed only weak or no responses to the compounds. These results suggest that TRPML3 in native cells might be absent from the plasma membrane or that the protein is a subunit of heteromeric channels that are nonresponsive to the activators identified in this screen.

INTRODUCTION

The TRPML subfamily of transient receptor potential (TRP) channels consists of the three proteins—TRPML1, TRPML2, and TRPML3—which were initially described in the wake of the discovery of the human mucolipin (*TRPML1*) gene as the cause of Mucolipidosis Type IV (Bargal et al., 2000). The murine *Trpml2* and *Trpml3* genes (mucolipin 2 and 3) were identified in a positional cloning project to identify the gene responsible for the murine varitint-waddler (*Va*) mutation (Di Palma et al., 2002). Ultimately, a single A419P amino acid substitution within the predicted transmembrane domain 5 (TM5) of murine TRPML3 was identified to cause the severe auditory, vestibular, and melanocyte phenotype: variegated coat color, circling behavior, deafness, and perinatal lethality observed in *Va*/*Va* homozygotes (Di Palma et al., 2002). The A419P substitution renders TRPML3 constitutively active (Grimm et al., 2007; Kim et al., 2007; Nagata et al., 2008; Xu et al., 2007), which has led to the hypothesis that constitutive activity leads to calcium overload and apoptotic cell death in cells that natively express TRPML3, such as melanocytes and sensory hair cells (Grimm et al., 2007, 2009; Kim et al., 2007; Nagata et al., 2008; Xu et al., 2007). Heterologously expressed TRPML3 displays currents that are inwardly rectified and regulated by extracellular [H^+] and [Na^+] (Kim et al., 2007; Kim et al., 2008). It has been hypothesized that luminal pH affects TRPML3 activity (Kim et al., 2008). Despite progress in characterizing wild-type and mutant TRPML3 isoforms, the physiological roles of this TRP ion channel remain unknown.

Selective ligands and activators are playing major roles in characterizing the physiological roles of many TRP channels. In contrast to the increasing number of ligands, activators, and, recently, antagonists for many TRP channels (for reviews see Patapoutian et al., 2009 and Ramsey et al., 2006), there are neither activators nor selective inhibitors known for members of the TRPML subfamily. A reasonable and efficient approach to identify small molecule ion channel modulators is through compound library screening. In this report, we describe the identification of the first selective small molecule TRPML3 activators by high-throughput screening. Maximal activation capability of the different compounds ranged from only a fraction to up to two times higher than the activity of the TRPML3 *Va* mutant channel isoform. Low extracellular sodium had a strong synergistic effect on compound activation, extending the activity range of TRPML3 over two orders of magnitude. Using the identified agonists as tools, we sought to activate TRPML3 in native cell types, such as sensory hair cells and melanocytes. Only one compound was able to elicit weak calcium influx into primary epidermal melanocytes, and none of the compounds was effective on neonatal cochlear hair cells. This surprising discrepancy between heterologous expression and native cells suggests that TRPML3 channels are either largely absent from the plasma membrane of hair cells and melanocytes, or that plasma membrane localization of the channel is being tightly regulated, or alternatively, that TRPML3 in melanocytes and hair cells contributes to heteromeric channels that lack responsiveness to the activators.

RESULTS

High-Throughput Screen Reveals TRPML3 Activators

To identify compounds that elicit a TRPML3-specific increase of $[Ca^{2+}]_i$, we conducted two parallel high-throughput screens with

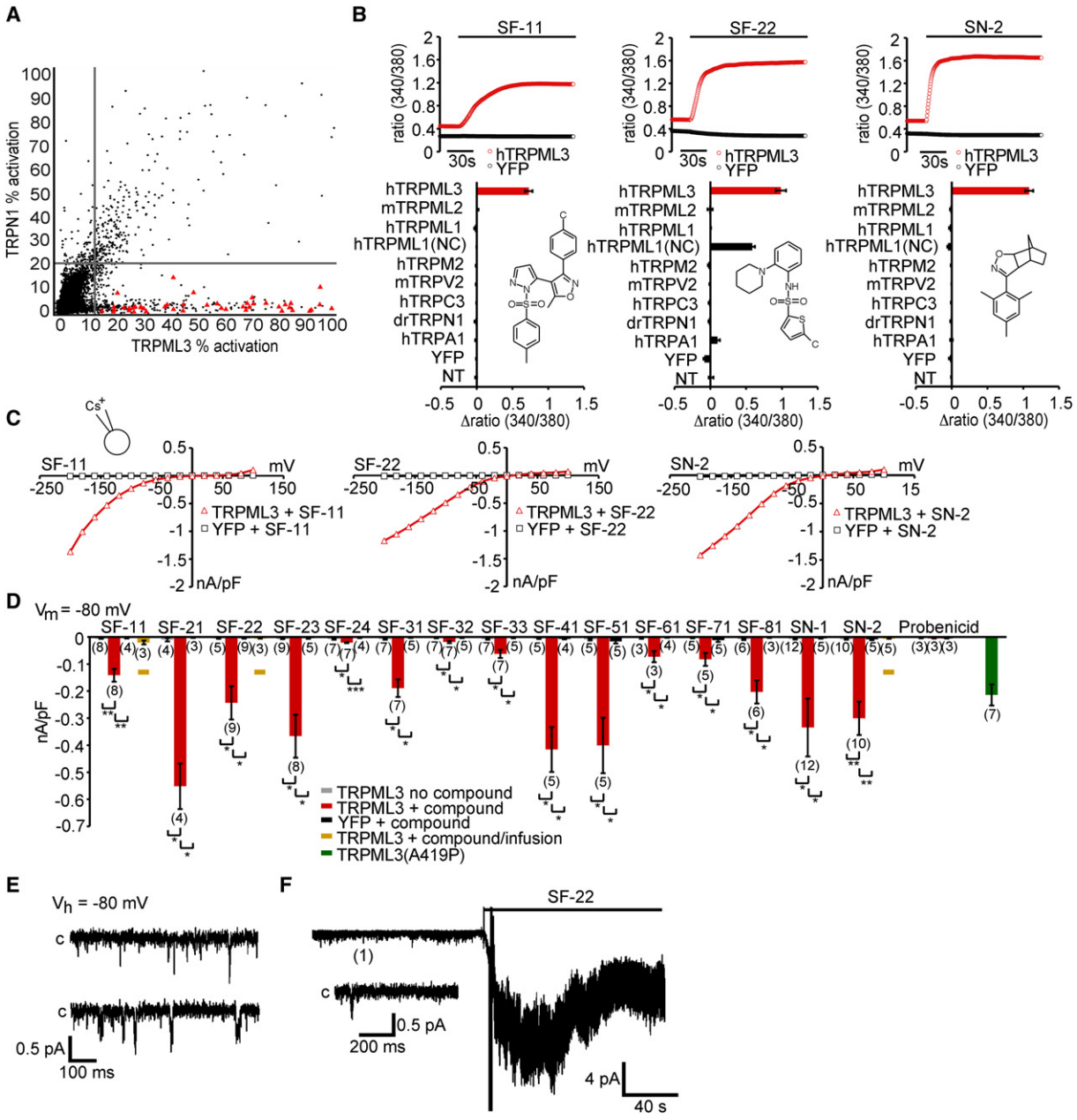

Figure 1. TRPML3-Activating Compounds

(A) Correlation plot for TRPML3 and TRPN1 high-throughput screens. Molecules found to be TRPML3-selective agonists are displayed as red triangles. Compound activity is normalized to the maximum carbachol response. Vertical and horizontal lines represent the hit cutoff values of the TRPML3 (11.46%) and TRPN1 (18.88%) screens.

(B) $[Ca^{2+}]_i$ increases of HEK293 cells transiently expressing human (h) TRPML3, or control TRP channels in response to application of 10 μM of selected compounds. TRPML1(NC) is a TRPML1 variant that is localized to the plasma membrane (see Figure 7A–C). For details and responses to compounds from all scaffold groups, see Figure S1.

(C) Steady-state current-voltage plots of whole-cell currents elicited in HEK293 cells transiently transfected with human TRPML3 or YFP (negative control) after perfusion with compounds SF-11, SF-22, and SN-2 (10 μM in standard bath solution). For details and responses to compounds from all scaffold groups, see Figure S2.

(D) Bar diagram shows average inward current densities at −80 mV of TRPML3-expressing HEK293 cells before (no compound) and after compound application (+ compound). Cells transfected with the constitutively active human TRPML3(A419P) isoform (green) were used as positive controls, and cells transfected with YFP were used as negative controls. In general, three bars are shown for each test series (no compound and with compound on TRPML3-expressing cells and with compound on YFP-expressing cells). For compounds SF-11, SF-22, and SN-2, we tested intracellular application (infusion), resulting in a fourth bar, shown and indicated in amber. Compound SF-11 elicited responses when applied intracellularly, which indicates that this molecule is either cell membrane permeant or that it is able to act on distinct intra- and extracellular activation sites. Compounds SF-22 and SN2 did not elicit a response when infused into the cells, indicating that the compounds act exclusively extracellularly, and suggesting that the compounds are not cell membrane permeable. The control compound probenicid did

HEK293 cells expressing TRPML3 or the unrelated TRPN1 protein. The screening conditions for high-throughput calcium flux screening, with Fluo-8 calcium indicator dye, were optimized to give the best balance between assay performance, reagent consumption, and suitability of the protocol for robotic-based screening (see Experimental Procedures). This process established precisely matched conditions for both screening campaigns. A total of 217,969 compounds were tested at a single concentration of approximately 3 μM. Compounds that activated TRPML3 or TRPN1 greater than the mean response plus three standard deviations (the hit cutoff) for the entire compound data set were considered as hits. A total of 632 compounds met this criterion for the TRPML3 campaign. Comparison to the TRPN1 control campaign established 300 compounds common to both campaigns (Figure 1A). Removal of overlapping hits left 332 TRPML3-selective agonist candidates. Triplicate retesting using the same assay conditions as the original screen confirmed 244 compounds with activity greater than the hit cutoff. Counter testing using TRPN1-expressing HEK293 cells revealed that 29 of these 244 candidates were active and, therefore, nonselective for TRPML3. Twenty-seven compounds were unavailable for further testing, which left 188 candidates for which dose-response relationships were determined over a range from 29.9 μM to 1.5 nM. Compounds chosen for further evaluation had an EC_{50} value of less than 3 μM for TRPML3 and greater than 29.9 μM for TRPN1, amounting to a ≥10-fold preference for TRPML3. Fifty-three compounds met these criteria (see Tables S1 and S2 available online). Cheminformatics analyses placed the 53 activators into nine chemical scaffolds (SF) and 20 singletons (i.e., compounds sharing no structural resemblance within all other dosed compounds). The nine chemotypes identified were (pyrazol-5-yl)isoxazole-benzenesulfonamides (SF-1), secondary arylsulfonamides (SF-2), tertiary arylsulfonamides (SF-3), sulfonylarylpiperazines (SF-4), 1-(2,2,4-trimethylquinolinyl)-alkylones (SF-5), spirobenzoannulene-arylpyrazolones (SF-6), t-butyl-3-methyl-4-(arylsulfonyl)-pyrazol-5-ols (SF-7), arylsulfonylpyridin-2-ones (SF-8), and t-butyl-3methyl-furan-2-carboxamides (SF-9).

Different Compounds Have Distinct TRPML3 Activation Profiles

For further evaluation in alternative assays, we selected at least one representative of each chemical scaffold and two singletons, SN-1 and SN-2. Criteria for this selection were low EC_{50} values for TRPML3 activation, low activation of TRPN1, and compound availability. SF-9 compounds were not tested because they were not commercially available. In total, 15 compounds were obtained from commercial vendors, verified by liquid chromatography-mass spectrometry, and reconfirmed in TRPML3 and TRPN1 activation assays. All 15 compounds confirmed activity in the TRPML3 assay with EC_{50} values of less than 5 μM, and in the case of SF-11, SF-21, SF-22, SF-31, and SN-1, the EC_{50} values were less than 1 μM (Table 1). Only compounds SF-21 and SF-51 exhibited significant activity against TRPN1. Both compounds were more active when tested from powders, which may reflect some minor decomposition in the high-throughput screening samples, which are stored as liquids.

The 15 compounds were further evaluated in calcium imaging and patch-clamp electrophysiology experiments. Selectivity was tested using HEK293 cells transfected with expression vectors for TRPML3, TRPML2, TRPML1, TRPM2, TRPV2, TRPC3, TRPN1, and TRPA1. All tested compounds elicited strong increases of intracellular calcium in TRPML3-transfected cells using fura-2 as the calcium indicator dye (Figure 1B; Figure S1). The strongest responses, amounting to ≥1.5-fold increase in the 340 nm/380 nm ratio, were obtained with compounds SF-21, SF-22, SF-23, SF-31, SF-41, SN-1, and SN-2. We also observed that compounds SF21, SF-41, and SN-2 elicited a much more rapid increase than did the other compounds, with SF-33 and SF-51 displaying the slowest kinetics. The benzosulfonamide probenicid (4-(dipropylsulfamoyl)benzoic acid), a compound structurally similar to several of the scaffolds identified by high-throughput screening, was used as negative control and did not elicit any responses (data not shown).

Three compounds, SF-21, SF-41, and SF-81, also elicited responses in HEK293 cells expressing TRPML2 (Figure S1). In contrast, no responses were observed in cells expressing TRPML1, which is not surprising because TRPML1 is predominantly located in lysosomes. When we tested the compounds on the mutant TRPML1(NC) isoform that is present in the plasma membrane (see below for details), we found that compound SF-22 was able to activate this channel. None of the compounds substantially activated any of the other TRP channels tested. The nonspecific responses of some compounds observed on TRPML2 and TRPML1(NC) confirmed that these two channels are localized in the plasma membrane of transfected HEK293 cells.

Whole-cell patch-clamp experiments revealed inwardly rectifying currents in TRPML3-transfected cells for all compounds, with average current densities between 20 and 600 pA/pF at −80 mV (Figure 1C; Figure S2). No significant currents were detectable in cells transfected with YFP only, or in cells expressing unrelated channels, such as TRPV2 or TRPA1 (data not shown). Average current densities in TRPML3 transfected cells perfused with compounds SF-22, SF-23, SF-31, SF-81, SN-1, and SN-2 were comparable to average current densities obtained from cells expressing the constitutively active varitint-waddler mutant isoform A419P of TRPML3 (Figure 1D) (Grimm et al., 2007). Stronger responses were obtained with compounds SF-21, SF-41, and SF-51. The combined results of the

not activate TRPML3. Statistical comparisons of means were made using one-way ANOVA followed by Tukey's post test (mean values ± SEM, number in parentheses are the number of cells analyzed). ***$p < 0.0001$, **$p < 0.001$, and *$p < 0.01$.

(E) Continuous sample traces demonstrate spontaneous TRPML3 single channel openings in an outside-out patch in the absence of the small molecule activator. "C" indicates the closed level of the traces.

(F) A representative outside-out patch recording is seen, illustrating the effect of compounds SF-22 on the activity of TRPML3 expressed in HEK293 cells. The patches were held at −80 mV. The compound was applied, as indicated by the bar. The inset below the recording shows the expanded sample trace from the same patch obtained before the application of SF-22.

Table 1. Summary of Data for the 15 TRPML3-Selective Activators

Compound ID (chemical name)	Max % Activation (TRPML3)	Max % Activation (Control)	EC_{50} (μM) (TRPML3)	EC_{50} (μM) (Control)	ΔF340/F380 (TRPML3)	ΔF340/F380 (Control)	nA/pF (−80 mV) (TRPML3)	nA/pF (−80 mV) (Control)
SF-11 (3-(4-chlorophenyl)-5-methyl-4-[2-(4-methylphenyl)sulfonylpyrazol-3-yl]-1,2-oxazole)	135 ± 20	8 ± 1	0.26 ± 0.04	>29.9	0.72 ± 0.05	−0.005 ± 0.002	−0.14 ± 0.02	−0.004 ± 0.001
SN-1 (N-tert-butyl-3-(3-tert-butyl-1-methyl-7-oxo-4H-pyrazolo[4,3-d]pyrimidin-5-yl)-4-ethoxybenzenesulfonamide)	151 ± 14	6 ± 0	0.88 ± 0.06	>29.9	1.15 ± 0.06	0.005 ± 0.004	−0.33 ± 0.10	−0.005 ± 0.001
SF-21 (4-chloro-N-(2-morpholin-4-yl cyclohexyl)benzenesulfonamide)	200 ± 7	61 ± 2	0.45 ± 0.04	14.24 ± 2.03	1.38 ± 0.10	0.033 ± 0.008	−0.55 ± 0.08	−0.003 ± 0.001
SF-22 (5-chloro-N-(2-piperidin-1-yl phenyl)thiophene-2-sulfonamide)	156 ± 16	1 ± 0	0.66 ± 0.06	>29.9	1.00 ± 0.07	−0.082 ± 0.014	−0.24 ± 0.06	−0.004 ± 0.001
SF-31 (1-(4-ethoxynaphthalen-1-yl) sulfonylazepane)	130 ± 20	2 ± 1	0.99 ± 0.23	>29.9	1.00 ± 0.10	−0.011 ± 0.001	−0.19 ± 0.03	−0.003 ± 0.001
SF-23 (5-chloro-N-(2-morpholin-4-yl phenyl)thiophene-2-sulfonamide)	174 ± 1	1 ± 1	1.10 ± 0.15	>29.9	0.93 ± 0.07	0.005 ± 0.005	−0.37 ± 0.08	−0.005 ± 0.001
SF-41 (1-(2,4-dimethylphenyl)-4-piperidin-1-yl sulfonylpiperazine)	138 ± 12	12 ± 1	2.11 ± 0.69	>29.9	0.99 ± 0.07	0.015 ± 0.001	−0.42 ± 0.07	−0.007 ± 0.002
SF-51 (2-[2-oxo-2-(2,2,4-trimethylquinolin-1-yl) ethyl]isoindole-1,3-dione)	175 ± 18	47 ± 3	0.93 ± 0.20	>29.9	0.78 ± 0.03	−0.007 ± 0.005	−0.41 ± 0.10	−0.016 ± 0.008
SF-32 (1-(4-ethoxy-2,3-dimethylphenyl) sulfonylpiperidine)	119 ± 5	2 ± 1	1.81 ± 0.14	>29.9	0.52 ± 0.05	−0.008 ± 0.005	−0.02 ± 0.01	−0.003 ± 0.001
SF-24 (4-methyl-N-(2-phenylphenyl) benzenesulfonamide)	86 ± 7	2 ± 0	2.41 ± 0.87	>29.9	0.51 ± 0.05	0.016 ± 0.023	−0.02 ± 0.01	−0.003 ± 0.001
SF-33 (5-chloro-N,N-diethyl-4-methyl-2-propoxybenzenesulfonamide)	119 ± 21	2 ± 1	4.79 ± 1.09	>29.9	0.65 ± 0.10	−0.007 ± 0.016	−0.06 ± 0.02	−0.003 ± 0.001
SN-2 (5-mesityl-3-oxa-4-azatricyclo [5.2.1.0∼2,6∼]dec-4-ene)	149 ± 11	3 ± 1	1.13 ± 0.16	>29.9	1.08 ± 0.05	−0.024 ± 0.012	−0.30 ± 0.07	−0.009 ± 0.003
SF-61 (4-(2-methoxyphenyl)spiro[3,4-dihydropyrazole-5,8′-6,7-dihydro-5H-benzo[7]annulene]-9′-one)	102 ± 22	2 ± 1	3.74 ± 1.02	>29.9	0.56 ± 0.03	−0.005 ± 0.006	−0.07 ± 0.01	−0.002 ± 0.001
SF-71 ([2-tert-butyl-5-methyl-4-(4-methylphenyl)sulfonylpyrazol-3-yl] butanoate)	85 ± 8	2 ± 1	2.52 ± 0.83	>29.9	0.75 ± 0.06	−0.002 ± 0.004	−0.08 ± 0.02	−0.012 ± 0.006
SF-81 (4,6-dimethyl-3-(2-methylphenyl) sulfonyl-1-propan-2-yl pyridin-2-one)	138 ± 21	1 ± 0	2.29 ± 0.19	>29.9	0.62 ± 0.05	−0.005 ± 0.016	−0.20 ± 0.03	−0.002 ± 0.001

Maximum activation is shown in percentage, normalized to the maximum carbachol responses, and EC_{50} values are reported as mean values ± SD ($n = 3$). Controls for activation and EC_{50} are TRPN1-expressing HEK293 cells. Fura-2 (ΔF340/F380) and patch-clamp data (nA/pF) are mean values ± SEM ($n \geq 3$). Controls for calcium imaging and patch-clamp experiments are YFP-expressing HEK293 cells.

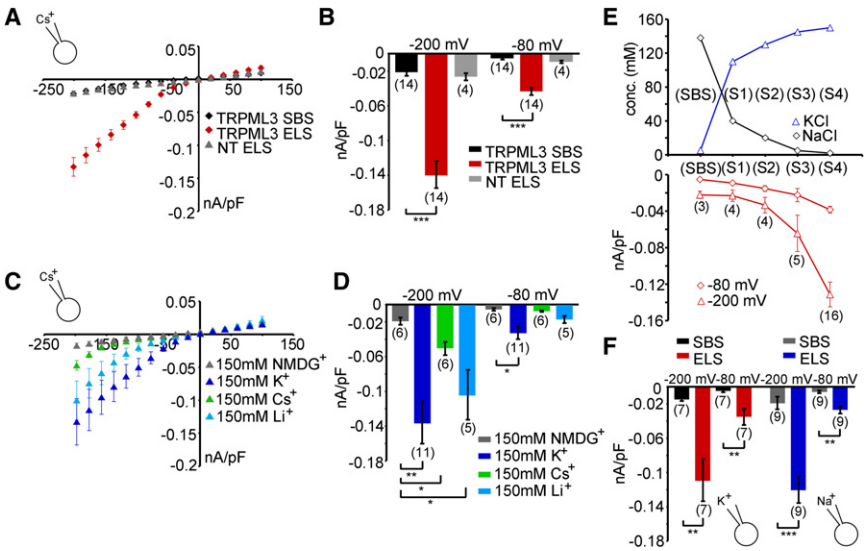

Figure 2. Effects of Extracellular Sodium on TRPML3

(A) Average steady-state current-voltage plots of whole-cell currents elicited in HEK293 cells expressing murine TRPML3 before and after perfusion with extracellular solution containing 2 mM NaCl, 150 mM KCl, 0.25 mM $CaCl_2$, 10 mM HEPES, and 10 mM D-glucose (pH 7.4) (endolymph-like solution [ELS]). Standard bath solution (SBS) contained 138 mM NaCl, 5.4 mM KCl, 2 mM $MgCl_2$, 2 mM $CaCl_2$, 10 mM HEPES, and 10 D-glucose (pH 7.4). The major cation in the pipette solution was 150mM Cs^+ (pH 7.2). Currents elicited with extracellular ELS in nontransfected HEK293 cells (NT) are depicted in gray.

(B) Average inward current densities of the experiments in (A) at −80 mV and −200 mV.

(C) Average steady-state current-voltage plots of whole-cell currents in presence of extracellular solution containing either 150 mM KCl, LiCl, CsCl, or NMDG-Cl (0 Ca^{2+}, 0 Mg^{2+}, 0 Na^+). The major cation in the pipette solution was 150 mM Cs^+ (pH 7.2).

(D) Average inward current densities of the experiments in C at −80 mV and −200 mV.

(E) "Dose-response" curve obtained from currents measured as described in A in different sodium and potassium concentrations corresponding to mouse endolymph composition during neonatal inner ear maturation (SBS = 138 mM NaCl and 5.4 mM KCl; S1 = 40 mM NaCl and 110 mM KCl; S2 = 20 mM NaCl and 130 mM KCl; S3 = 5 mM NaCl and 145 KCl; and S4 = 2 mM NaCl and 150 mM KCl).

(F) Average inward current densities before and after perfusion with ELS at −80 mV and −200 mV. The major cation in the pipette solution was either K^+ or Na^+ (150 mM [pH 7.2]), as indicated. Shown are mean values ± SEM (*n* = parenthesized). Statistical comparisons of means were made using one-way ANOVA followed by Tukey's post test; ***$p < 0.0001$, **$p < 0.001$, and *$p < 0.01$.

high-throughput screen, the fura-2 calcium imaging confirmation studies, as well as the whole-cell patch-clamp data are summarized in Table 1.

Excised patch experiments were performed to further confirm the ability of selected compounds (SF-22, SF-23, and SN-2) to activate TRPML3. In general, channel density was too high to clearly distinguish single channels, but the recordings confirmed that the tested compounds markedly increased TRPML3 activity (Figures 1E and 1F). We estimate that the conductance of TRPML3 channels, when activated with 10 μM SN-2, is approximately 10 pS at −80 mV, which is comparable to previously observed values (Xu et al., 2007).

In summary, all 15 candidate compounds identified in the high-throughput screen were able to activate TRPML3. Differences between the compounds include different maximal response levels and different apparent activation kinetics, as well as some of the compounds being able to activate the related TRPML1 and TRPML2 channels.

Low Extracellular Na^+ Concentration Increases the Open Probability of TRPML3 and Potentiates Compound Effects

Recently, it has been shown that high extracellular sodium has an inhibitory effect on the activity of wild-type TRPML3 (Kim et al., 2008). This is an intriguing finding because, in the inner ear, TRPML3 is transiently detectable at the base of mouse cochlear hair cell stereocilia between postnatal days 2–6 (P2-P6). Between P6 and P10, the protein is down-regulated and at P10, it is no longer detectable in the apical hair cell membrane by immunocytochemistry (Atiba-Davies and Noben-Trauth, 2007; van Aken et al., 2008). The transient expression of TRPML3 in stereocilia correlates with a critical period of organ of Corti maturation in which hair and supporting cells acquire their mature cytomorphologies, hair cells become mechanosensitive (Waguespack et al., 2007), and afferent and efferent innervation assume their adult patterns (Simmons et al., 1996). Likewise, the extracellular solution of the scala media, the endolymph, acquires its typical composition of low Na^+ (from 36 mM at P1, to 4.1 mM at P5, to 2.8 mM in the adult mouse) and high K^+ (from 104 mM at P1, to 136 mM at P5, to 202 mM in the adult) (Yamasaki et al., 2000). In particular, the changes in endolymph composition during a period of strong TRPML3 expression in the hair bundle spurred our interest to investigate whether TRPML3 displays altered activity when exposed to endolymph-like solutions in comparison with standard bath solution.

We found that, in the presence of endolymph-like extracellular solution (ELS) with high K^+ (150 mM) and low Na^+ (2 mM), TRPML3-expressing HEK293 cells showed a robust inwardly rectifying current (Figures 2A and 2B) that was not detectable when the cells were exposed to standard bath solution (SBS) containing high Na^+ (138 mM). Extracellular solution containing either K^+ or Li^+ as the sole cation (at 150 mM) evoked currents of comparable sizes in wild-type TRPML3-expressing HEK293 cells (Figures 2C and 2D). Peak currents at −200 mV varied between 100 pA/pF and 130 pA/pF. Extracellular solution containing 150 mM Cs^+ resulted in significantly smaller inward currents, with peak currents at −200 mV of about 50 pA/pF. TRPML3 was impermeable to the organic monovalent cation N-methyl-D-glucamine ($NMDG^+$). Because the composition of endolymph is changing during development (Yamasaki et al., 2000), we tested different solutions (S1–S4) containing varying concentrations of K^+ and Na^+. Solutions S1–S4 correspond to the potassium and sodium concentrations obtained from P1, P3, P5, and adult mouse endolymph (Yamasaki et al., 2000).

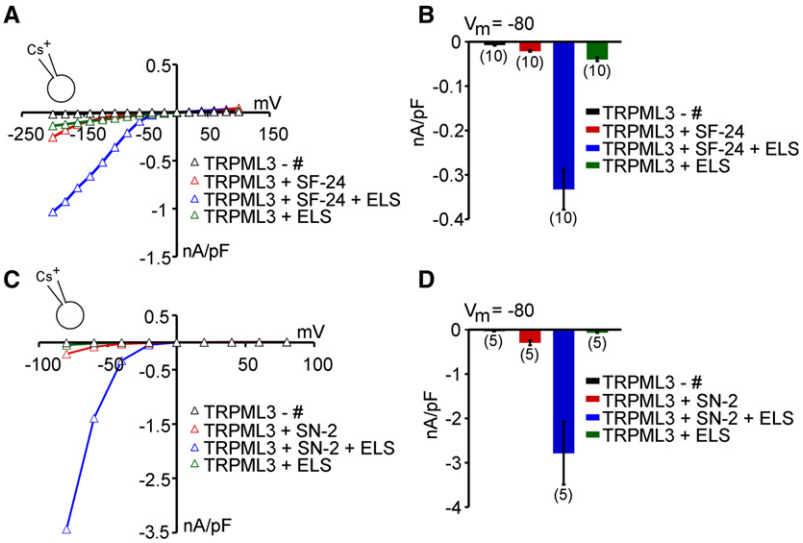

Figure 3. Low Extracellular Sodium Potentiates Agonist Effects on TRPML3

(A) Representative steady-state current-voltage plots of whole-cell currents before and after perfusion with compound SF-24 alone (10 μM), compound SF-24 + ELS, and with ELS alone.

(B) Average inward current densities at −80 mV of experiments as shown in (A), normalized by cell capacitance (pF). Shown are mean values ± SEM (*n* = number of cells analyzed).

(C and D) Same experiments as described in (A and B) with singleton compound SN-2 (10 μM), holding potential = +10 mV, voltage steps between −80 mV and + 80 mV.

We found an increase of TRPML3 current densities with decreasing sodium and increasing potassium concentrations (Figure 2E).

An increase of calcium (up to 2 mM) or adding magnesium (2 mM) to ELS did not significantly change the previously observed effects. Likewise, omission of divalents in SBS had no effect. Increasing the BAPTA concentration in the pipette solution from 1 mM to 10 mM also had no significant effect (data not shown). These results are consistent with the finding that TRPML3 activity depends on the extracellular Na^+ concentration, as reported elsewhere (Kim et al., 2008). TRPML3 is closed at the physiologically high extracellular Na^+ concentration of 138 mM (SBS), but it shows increased open probability when [Na^+] falls below 20 mM.

To determine whether changes in the intracellular ionic composition interfere with the activity of TRPML3, we replaced the cesium-containing pipette solution with solutions containing 150 mM K^+ or 150 mM Na^+, respectively. With either ion, we observed no significant differences in the current densities elicited by ELS (peak currents between 100 pA/pF and 130 pA/pF at −200 mV), compared with measurements with cesium inside the patch pipette (Figure 2F). These results show that, in contrast to high extracellular sodium, high intracellular sodium does not block TRPML3 activity.

We next investigated the relationship between activation with ELS and activation with compound activators. We perfused TRPML3-expressing HEK293 cells with a series starting with compound alone (in SBS), with compound in ELS, and finally with ELS alone. Two representative compounds, SF-24 and SN-2, were tested. SF-24 is one of the least effective compounds, and SN-2 is one of the most active ones. Combining SF-24 with ELS had a strong synergistic effect on TRPML3 activation, resulting in up to 10-fold increases in current densities, when compared to ELS alone or SF-24 in SBS (Figures 3A and 3B). SN-2 had a similar synergistic effect, also reaching up to 10-fold enhancement of the combined response when compared with the individual responses, reaching average current densities of up to 3 nA/pF at −80 mV (Figures 3C and 3D).

Cochlear Hair Cells Expressing TRPML3 Do Not respond to ELS and Compound Activators

Neonatal hair cells express TRPML3, and the channel protein is detectable in mouse cochlear hair cell stereocilia during the first weeks after birth (Di Palma et al., 2002; van Aken et al., 2008). In varitint-waddler mutant hair cells, constitutively active TRPML3 leads to calcium loading and death of cochlear hair cells, which suggests that at least a subpopulation of TRPML3 channels are located in the plasma membrane of hair cells (Grimm et al., 2007, 2009; Kim et al., 2007; Nagata et al., 2008; Xu et al., 2007). This expression in vivo raised the question whether ELS or compound activators or combinations of both are able to activate TRPML3 in native hair cells. We acutely isolated P5-P6 rat organ of Corti and we tested their response to ELS, and SF-21 or SN-2 in SBS, as well as SN-2 in ELS. Neither compound at concentrations of up to 100 μM, with or without endolymph-like extracellular solution, elicited TRPML3 channel activity in cochlear hair cells (Figure S3). Mechanotransduction currents in all cells tested were unperturbed by ELS or compound exposure, or combinations of both (data not shown).

Epidermal Melanocytes Expressing TRPML3 Show No or Only Small Responses to Compound Activators

The varitint-waddler phenotype also revealed that melanocytes of the epidermis express mutant TRPML3 in the plasma membrane, leading to calcium loading and cell death (Di Palma et al., 2002). We examined primary human epidermal melanocytes, which express all three TRPML channels (Figure 4A), and we tested compounds at concentrations up to 100 μM. The compounds elicited no or very small responses, with the exception of SN-2, which, when applied at concentrations of 30 μM and 100 μM, elicited a stronger response (Figure 4B). NIH 3T3 cells, which do not express TRPML3 natively (Figure 4C), were used as a negative control, and none of the compounds tested at 100 μM elicited a response (Figure 4D). When we overexpressed TRPML3 in melanocytes, we detected strong increases of $[Ca^{2+}]_i$ after compound application, similar to the responses observed in HEK293 cells (Figure 4E). Overexpression of TRPML3 in NIH 3T3 cells resulted in responses comparable to the effects of compounds on TRPML3-expressing HEK293 cells or melanocytes overexpressing TRPML3 (Figure 4F).

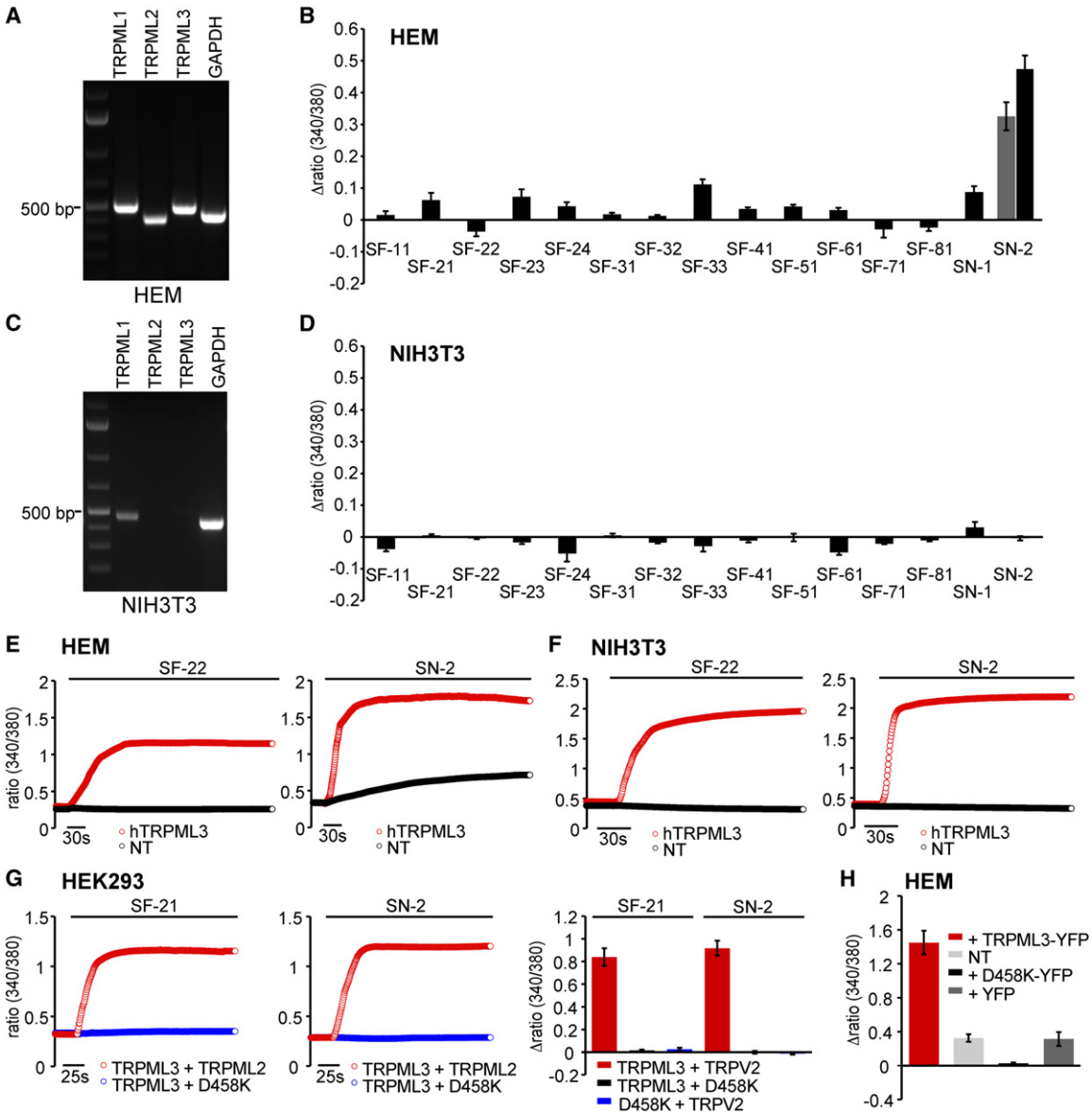

Figure 4. Compound Effects on Epidermal Skin Melanocytes

(A) RT-PCR shows robust expression of TRPML1 (500 bp), TRPML2 (411 bp), TRPML3 (487 bp), and GAPDH control (444 bp) in primary human epidermal melanocytes (HEM).

(B) Ca^{2+}-imaging results showing changes of $[Ca^{2+}]_i$ in HEM in response to application of TRPML3-activating compounds at concentrations of 100 μM (mean values ± SEM; $n \geq 3$ independent experiments with 20–30 cells). Responses to SN-2 are shown for 30 μM (gray bar) and 100 μM.

(C) RT-PCR demonstrating presence of TRPML1 (470 bp) and GAPDH (442 bp) transcripts in NIH 3T3 cells, but not TRPML2 (500 bp) and TRPML3 (550 bp).

(D) Ca^{2+}-imaging experiments as described in (B) showing compound effects (at 100 μM) on NIH 3T3 cells.

(E) Ca^{2+}-imaging experiments showing $[Ca^{2+}]_i$ increases in HEM transfected with human TRPML3-YFP or nontransfected cells (NT) upon application of SF-22 and SN-2 at 100 μM.

(F) Ca^{2+}-imaging experiments as described in (E) showing compound effects on NIH 3T3 cells transfected with human TRPML3-YFP or NT.

(G) Ca^{2+}-imaging experiments on HEK293 cells expressing TRPML3 and dominant negative TRPML3(D458K) or TRPML2 as a control. Shown are responses to compounds SF-21 and SN-2.

(H) SN-2-elicited changes of $[Ca^{2+}]_i$ in HEM transfected with expression vectors for TRPML3, dominant negative TRPML3(D458K), and YFP control. NT, nontransfected control cells.

These results suggest that TRPML3 might not be present in the plasma membrane of hair cells and is also largely absent from the plasma membrane of primary melanocytes, or that the channel might be in a state that renders it nonresponsive to most compounds. The effect of SN-2 on melanocytes raised the question whether this compound acts nonspecifically, which would be surprising because it did not show any activity on other TRP channels, not even the related TRPML2 and TRPML1(NC)

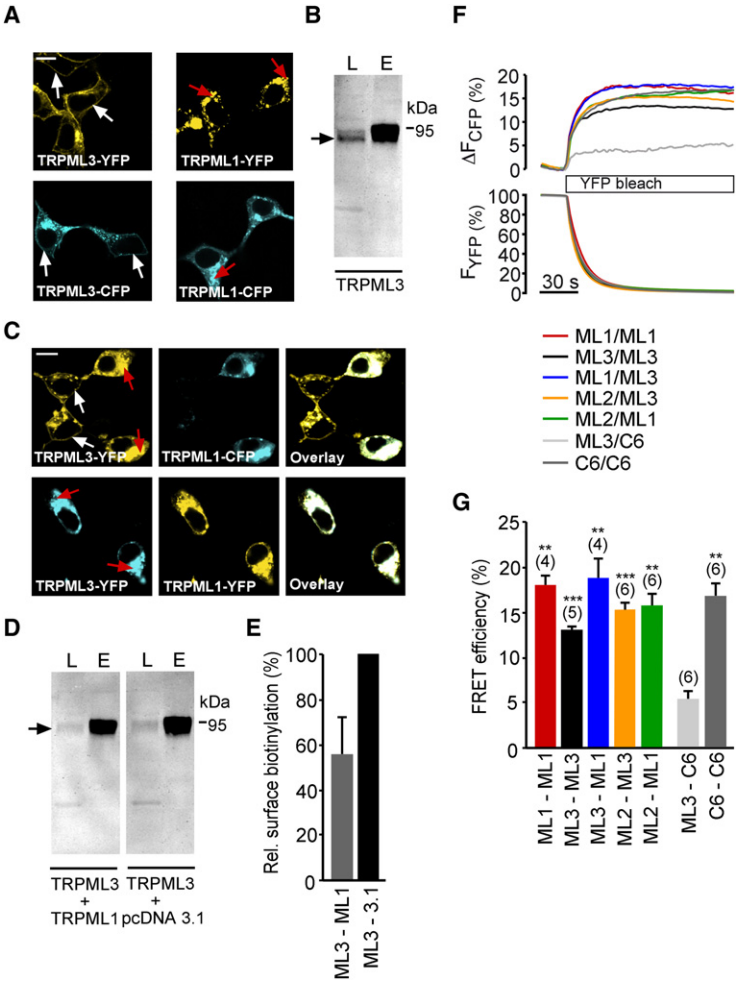

Figure 5. Interactions Between Different TRPML Channels

(A) Confocal images of HEK293 cells expressing human TRPML3-YFP or -CFP as well as human TRPML1-YFP or -CFP. White arrows indicate plasma membrane and red arrows indicate intracellular protein aggregations.

(B) Surface biotinylation experiment showing human TRPML3-YFP in the plasma membrane. L = input load (1% of total), E = elution from streptavidin beads. Surface-biotinylated YFP-tagged TRPML3 was visualized with anti-GFP antibody (Clontech, JL8).

(C) Subcellular localization of human TRPML3-YFP when coexpressed 1:1 with human TRPML1-CFP in HEK293 cells and vice versa.

(D) Biotinylation experiments showing human TRPML3-YFP (arrow) coexpressed with either human TRPML1 1:1 or empty vector control in HEK293 cells visualized with anti-GFP antibody in western blot.

(E) Relative surface biotinylation of TRPML3 coexpressed with TRPML1 in percentage (mean ± SEM, n = 4). Cotransfections with empty vector were set to 100%.

(F) Fluorescence energy resonance transfer (FRET) experiments showing average FRET efficiencies between TRPML homo- and heteromers. FRET efficiencies were determined by measuring the recovery of CFP fluorescence during YFP photobleaching. Cells were excited at 410 nm and 515 nm for CFP and YFP detection, respectively. YFP was bleached with an illumination at 512 nm for 2.2 s.

(G) Average FRET efficiencies reported as mean values ± SEM (n = parenthesized). ***p < 0.0001 and **p < 0.001, Student's t test, unpaired, comparison with TRPC6/TRPML3 coexpression as negative control. All scale bars = 15 μm.

isoform (Figure 1B). Because SN-2 is not cell permeant (Figure 1D), we argue that its action on melanocytes is based on an interaction with an extracellular site. To further investigate this, we utilized the dominant negative TRPML3(D458K) mutant (Kim et al., 2009), which completely eliminates responses to activators when coexpressed with TRPML3 in HEK293 cells (Figure 4G). Dominant negative TRPML3(D458K) was highly effective in eliminating SN-2-induced activity in epidermal melanocytes (Figure 4H), suggesting that SN-2 activates a channel that is not responsive in presence of TRPML3(D458K). Such a dominant negative action might be attributed to potential heteromerization of TRPML3(D458K) with an SN-2-responsive channel. Although in a different context, heteromerization of TRPML channels has previously been postulated (Kim et al., 2009; Venkatachalam et al., 2006; Zeevi et al., 2007, 2009), and particularly TRPML1 has been put forward as a regulator of the plasma membrane concentration of TRPML3 (Venkatachalam et al., 2006), although the physiological relevance of this in vitro observation is very much dependent on the circumstances, cell type, and perhaps other unknown factors (Kim et al., 2009).

TRPML Channels Form Heteromers

Coexpression of TRPML1 strongly decreases compound responsiveness of TRPML3 in transfected HEK293 cells. To confirm the previously postulated in vitro trafficking effects of TRPML1 on TRPML3, and to demonstrate that these effects are indeed the result of heteromerization, we differentially tagged the two proteins with YFP and CFP. HEK293 cells transiently transfected with TRPML1-YFP or -CFP and TRPML3-YFP or -CFP alone showed predominant expression of TRPML1 in intracellular compartments, whereas TRPML3 was detected in intracellular vesicles as well as in the plasma membrane (Figure 5A). Plasma membrane localization of TRPML3 in transfected HEK293 cells was confirmed by surface biotinylation, pull down of biotinylated proteins, and western blot (Figure 5B). When TRPML1 was coexpressed with TRPML3, the subcellular localization of TRPML3 changed: more overexpressed TRPML3 protein was visible in intracellular compartments where it overlapped with TRPML1. Nearby cells that did not express TRPML1 still showed plasma membrane localization of TRPML3 (Figure 5C). In addition, surface biotinylation experiments revealed a relative decrease of TRPML3 plasma membrane expression in cells coexpressing both proteins, compared with control experiments with empty vector cotransfection. The amount of TRPML3 in the plasma membrane, when cotransfected with control vector, was 25.8 ± 4.2% (mean ± SEM) of total TRPML3 protein (n = 3). Coexpression of TRPML1 decreased the amount of TRPML3 detectable in the plasma membrane by 44.7 ± 16.0% (mean ± SEM; n = 4) (Figures 5D and 5E). These results show that TRPML1 coexpression is able to reduce the amount of TRPML3 protein in the plasma membrane of HEK293 cells. Because not all cells are transfected equally and surface biotinylation averages across all cells, it is clear that this experiment only provides

an indication of a potential functional interaction between TRPML1 and TRPML3 in this heterologous expression system.

To demonstrate that these effects are caused by direct interaction of the two proteins (i.e., heteromerization), we performed fluorescence resonance energy transfer (FRET) experiments with the respective TRPML-CFP and -YFP fusion proteins. We measured average FRET efficiencies between 13% and 20% for TRPML homomers and heteromers, indicative of close proximation of the two fluorophores (Figures 5F and 5G). FRET effects between TRPC6 and TRPML3 showing an average FRET efficiency of 5% were regarded as nonspecific and comprised our negative control. TRPC6 homomers displayed an average FRET efficiency of 17%. This finding is in accordance with FRET efficiencies previously described for heteromeric TRPML channels and TRPC6 (Hofmann et al., 2002; Venkatachalam et al., 2006). Overall, these results show that all TRPML channels are able to heteromerize with each other. Although these findings are based on overexpression studies, we believe that heteromerization could be happening in cells and tissues where the different TRPML channels are coexpressed (Figure S4), although coexpression does not necessarily mean that the channels are targeted to the same subcellular locations (Kim et al., 2009; Zeevi et al., 2009).

On the basis of this confirmation of TRPML1 and TRPML3 interactions, we tested whether coexpressed TRPML1 affects the ability of TRPML3 to respond to compound activation. With all four compounds tested (SF-21, SF-22, SF-23, and SN-2), we observed a strong reduction of the calcium imaging responses when TRPML1 was coexpressed (Figures 6A–6C). Coexpression of TRPML2 or TRPV2 did not show any decrease of TRPML3 responsiveness. Whole-cell patch-clamp recordings confirmed these results (Figures 6E–6G). Interestingly, TRPML1 was not able to suppress the constitutively active TRPML3 varitint-waddler mutant isoforms Va and Va^{J}. Coexpression of these isoforms with TRPML1 in a ratio 1:1 and even 1:5 still revealed highly elevated intracellular calcium levels (Figure S5). This result suggests that in varitint-waddler animals, mutant TRPML3 channels might be mislocalized to the plasma membrane as a result of the inability of TRPML1 to affect trafficking. The mechanism of this effect, however, is not clear.

We further investigated the effect of TRPML1 on trafficking of TRPML3 by making use of TRPML1 mutants that locate to the plasma membrane instead of endosomes/lysosomes. This can be achieved by removal of both TRPML1-specific dileucine motifs (lysosomal targeting sites [LTSs]) in the N and C termini (Miedel et al., 2006; Venkatachalam et al., 2006; Vergarajauregui and Puertollano, 2006) (Figures 7A and 7B). The resulting TRPML1(NC) mutant isoform is expressed in the plasma membrane (Figure 7C) where it can be activated by compound SF-22 (Figure 1B), which is not cell permeable (Figure 1D). These results show that TRPML1(NC) is at least partially targeted to the plasma membrane and that the channel is functional.

Accordingly, coexpression of TRPML3 with TRPML1(NC) should result in a smaller reduction of TRPML3 responses upon compound application than coexpression with wild-type TRPML1. We found that coexpression of TRPML1(NC) indeed showed higher response levels upon agonist application than did coexpression with wild-type TRPML1 (Figures 7D–7F). Generally, these data corroborate the hypothesis that interaction

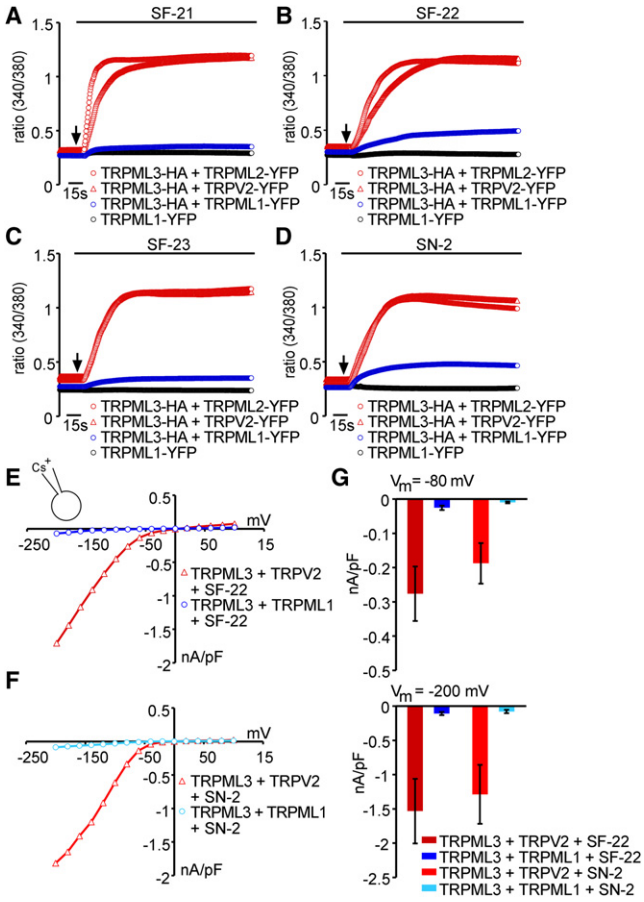

Figure 6. Coexpression of TRPML1 with TRPML3 Decreases Activation Effect of TRPML3 Agonists in Transfected HEK293 Cells

(A–D) Ca^{2+}-imaging measurements of $[Ca^{2+}]_i$ changes in HEK293 cells coexpressing TRPML3 with either TRPML1, TRPML2 (control), TRPV2 (control), or expression of TRPM1 alone in response to compounds SF-21, SF-22, SF-23, or SN-2 (10 μM). Shown are mean values ± SEM ($n \geq 3$ independent experiments with 20–30 cells each).

(E and F) representative steady-state current-voltage plots of whole-cell currents. Currents were elicited in HEK293 cells coexpressing TRPML3-YFP with either TRPML1-HA or TRPV2-HA (control) before and after perfusion with selected compounds (10 μM in SBS).

(G) Average inward current densities at −80 mV and −200 mV of experiments shown in (E and F).

with TRPML1 generates TRPML3/TRPML1 heteromers that preferentially localize to intracellular compartments. The question is whether this interaction is relevant in cells that natively express TRPML3.

We sought to further confirm this regulation by suppressing the expression of native TRPML1 in epidermal melanocytes. For this, we used a specific shRNA that is able to strongly down-regulate overexpressed human TRPML1 (Samie et al., 2009; Figure 7G). In native cells, however, overexpression of shRNA to TRPML1 did not affect responsiveness (Figure 7H), indicating that native TRPML1 expression is either too strong for efficient suppression with shRNA or that the lack of TRPML3 responsiveness in native cells is due to additional mechanisms independent of TRPML1. The latter hypothesis is supported by

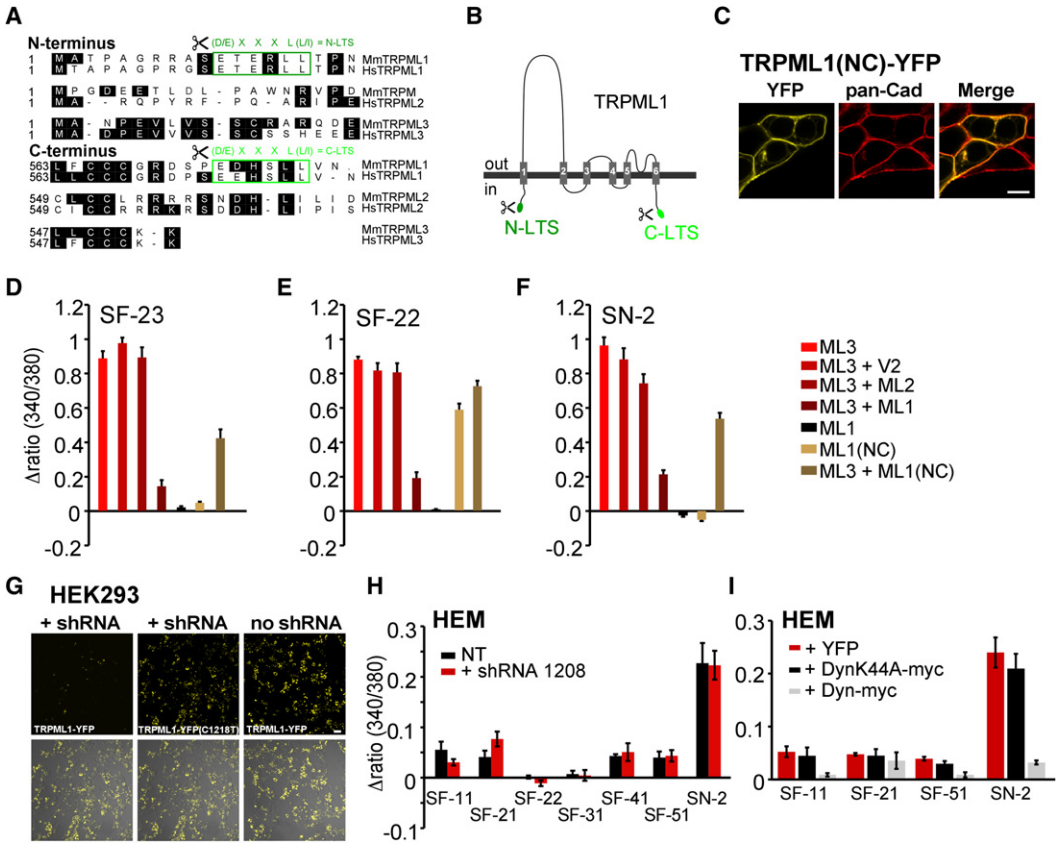

Figure 7. Effects of Modulating TRPML1 Expression and Modulation of Endocytosis on TRPML3 Agonist Responses

(A) Protein sequence comparison of the N and C termini of TRPML channels. Different lysosomal targeting sequence (LTS) motifs are labeled in green.

(B) Simple drawing of the TRPML1 topology indicating the positions of the LTS motifs that were removed in mutant (-LTS) TRPML1 isoforms.

(C) Representative laser scanning micrograph of HEK293 cells overexpressing TRPML1(NC)-YFP lacking N- and C-terminal LTS motifs. Please see Figure 5A for comparison with wild-type TRPML1 localization. The plasma membrane is visualized with pan-Cadherin (pan-Cad) antibodies (red). Scale bar = 10 μm.

(D–F) Ca^{2+}-imaging results showing relative $[Ca^{2+}]_i$ increases after application of compound SF-23, SF-22, or SN-2 in HEK293 cells coexpressing TRPML3 with TRPML1, with TRPML1(NC) or with various controls. Shown are mean values ± SEM ($n \geq 3$ independent experiments with 20–30 cells each).

(G) Confocal micrographs of HEK293 cells overexpressing wild-type TRPML1-YFP or TRPML1-YFP mutant (C1218T, silent mutation disrupting the shRNA binding region) in presence or absence of TRPML1 shRNA (shRNA 1208). Only wild-type TRPML1, but not the mutant is specifically down-regulated by shRNA 1208. Scale bar = 50 μm.

(H) Ca^{2+}-imaging results showing $[Ca^{2+}]_i$ increases in primary human epidermal melanocytes (HEM, black = nontransfected (NT)), and HEMs cotransfected with shRNA to TRPML1 (red) upon application of selected TRPML3 activating compounds from 5 different scaffolds (SF-11, -21, -22, -31, -41, and -51) and singleton SN-2 at 30 μM (mean values ± SEM, $n \geq 3$ independent experiments with 5–10 cells). An expression vector for YFP was cotransfected with the shRNA for identification of the transfected cells.

(I) Ca^{2+}-imaging results showing changes in $[Ca^{2+}]_i$ in HEMs transfected with either Dyn, DynK44A, or YFP (control) in response to application of TRPML3-activating compounds SF-11, SF-21, SF-51, and singleton SN-2 at a concentration of 30 μM, each (mean values ± SEM; $n \geq 3$ independent experiments with 20–30 cells).

recent reports arguing that colocalization of TRPML1 and TRPML3 in vivo only accounts for a small fraction of the channel populations (Kim et al., 2009; Zeevi et al., 2009).

Effect of Endocytosis Modulation on TRPML3 Compound Responses

Beside a possible regulation of TRPML3 plasma membrane localization by TRPML1, other plausible regulation mechanisms have recently been explored (Kim et al., 2009). The authors found that a dominant-negative dynamin mutant (DynK44A) increased plasma membrane expression of TRPML3, which led them to conclude that TRPML3 recycles between the plasma membrane and intracellular compartments via a dynamin-dependent endocytic pathway. On the basis of this finding, we would expect that increase of dynamin-mediated endocytosis would decrease the number of TRPML3 channels in the plasma membrane, whereas inhibition of dynamin would increase responsiveness to TRPML3 activators. To test this hypothesis, we coexpressed wild-type dynamin with TRPML3 in HEK293 cells. We indeed found a reduction in response to weak and strong TRPML3 activators, compared with control experiments (SF-24 and SN-2; Figure S6). When we repeated the experiment in epithelial melanocytes, we also found a reduction of the response to SN-2 (Figure 7I), indicating that the responding channel is affected by increased endocytosis. Conversely, when we coexpressed the dominant-negative K44A dynamin isoform with TRPML3 we

consistently found small response increases in HEK293 cells. When we expressed the K44A isoform in epithelial melanocytes, we did not, however, detect any significant changes in response levels to TRPML3 activating compounds (Figure 7I). The fact that neither TRPML1 knockdown nor block of dynamin-mediated endocytosis appeared to significantly modulate responses in cells natively expressing TRPML3, suggested that these manipulations were either not strong or sufficient enough or that alternative mechanisms are involved in the regulation of TRPML3 function.

DISCUSSION

In this study, we identified and confirmed 53 selective small molecule activators of TRPML3. Although the majority of the compounds were sulfonamides, they displayed a wide variety of structures belonging to nine chemical scaffolds and 19 singletons. We further analyzed 15 compounds in detail and found that their maximal activation capacities varied over an order of magnitude, indicating a variety of potential mechanisms of affecting TRPML3 activity. The combined collection of so many different but efficient activators of a single TRP channel is unprecedented, which provides an unparalleled set of novel tools to study the biophysical and physiological features of TRPML3.

Toward these goals, we analyzed the relationship between compound activation and regulation of the channel by extracellular Na^+. A previous study implicated Na^+ as a TRPML3 regulator, but not as a blocker per se (Kim et al., 2007). We found this feature intriguing because TRPML3 has been reported in the apical plasma membrane of sensory hair cells in the mouse cochlea during the first neonatal week (Atiba-Davies and Noben-Trauth, 2007; Di Palma et al., 2002; van Aken et al., 2008), a time period that coincides with changes of the ionic composition of the endolymph, the extracellular solution of the cochlear scala media into which the mechanosensitive stereociliary hair bundles protrude. Between birth and P5, when the expression of TRPML3 at the base of hair cell stereocilia is at its highest, the endolymphatic [Na^+] drops from 36 mM to 4.1 mM. Adult murine endolymph is composed of 2.8 mM Na^+ and 202 mM K^+ (Yamasaki et al., 2000). When we exposed TRPML3-expressing HEK293 cells to endolymph-like solutions, we detected a robust inward rectifying current whose maximal amplitudes were dependent on the extracellular Na^+ concentration. Specifically, TRPML3 activated when [Na^+] dropped below 20 mM and its activation was gradually more efficient when the [Na^+] was stepwise lowered to 2 mM, which elicited the maximal response. This concentration range matches the [Na^+] concentration changes during the neonatal maturation of cochlear endolymph (Yamasaki et al., 2000), and it raised two questions: first, whether lowering extracellular [Na^+] affects compound responsiveness and, second, whether neonatal hair cells are responsive to ELS and compound activation.

To answer the first question, we applied compounds in low extracellular [Na^+], and we detected a strong synergism that was obvious both with low-efficient compounds as well as with compounds that elicited strong responses. Our data confirmed that Na^+ is not a blocker of TRPML3 per se because compound activation happens in high extracellular Na^+ (138 mM). Nevertheless, lowering [Na^+] to 2 mM led to a 10-fold increase of the current response, a clear indication that the two activation mechanisms are cooperatively acting on TRPML3.

To investigate the second question of whether cochlear hair cells are able to utilize TRPML3 to detect changes of the ionic composition of endolymph, we exposed acutely isolated cochlear hair cells to ELS, compound activators, and to combinations of both. To our surprise, we were not able to elicit any TRPML3 responses when we exposed P4-P6 cochlear hair cells to ELS and to some of the most effective TRPML3 activators, even at very high compound concentrations. Application of compounds in ELS also did not elicit responses from sensory hair cells. Because the temporal expression pattern of TRPML3 in the rat cochlea could differ from the mouse, we also tested a total of 145 inner and outer hair cells from younger (P0) and older (up to P12) animals by puffing ELS onto their apical surface, but we did not observe specific responses (data not shown).

Albeit puzzling, these results reveal a number of interesting scenarios. One possibility is that TRPML3 is not present in hair cell plasma membranes. If this were the case, the varitint-waddler phenotype (Di Palma et al., 2002; Grimm et al., 2009) would have to be caused by mislocalization of the constitutively active TRPML3 *Va* isoform to the plasma membrane. A second possibility is that the activators that we identified act only on homomeric TRPML3 channels and that these homomeric channels only form when TRPML3 is overexpressed. In hair cells, TRPML3 would be a subunit of a more complex channel of unknown composition that is nonresponsive to the compounds. Third, plasma membrane–bound TRPML3 could be very tightly regulated and endocytotic removal of the channel from the plasma membrane renders hair cells nonresponsive.

A second cell type that natively expresses TRPML3 is epidermal melanocytes, which are more suitable for in vitro inquires than sensory hair cells. When we tested primary epidermal melanocytes, we were unable to evoke TRPML3 responses with all compounds except for SN-2, which at elevated concentrations was able to prompt a significant increase of the intracellular Ca^{2+} concentration. Because primary epidermal melanocytes can be transfected with expression plasmids, we first tested whether melanocytes have an inherent inability to respond to activators. This is not the case because when we transfected human melanocytes with a TRPML3 expression vector, we were able to measure with calcium indicator dyes robust responses of the transfected cells to compounds. A second question is whether TRPML3 is modified or regulated in native cell types rendering the channel nonresponsive. Phosphorylation or other forms of posttranslational modification could affect overexpressed TRPML3 channels. In such cases, we would not be able to detect strong responses to TRPML3 activators. It is therefore unlikely that TRPML3 in melanocytes is nonresponsive because of posttranslational modifications. Another form of regulation, heteromerization, relies on the endogenous expression of other channel proteins capable of interacting with TRPML3, resulting in heteromeric channels that might localize to intracellular compartments or do not respond to compound and ELS activation. We detected expression of TRPML1 and TRPML2 mRNA in the inner ear and in epidermal melanocytes, which would make heteromerization

with TRPML1 or TRPML2 a possibility in these cell types. Nevertheless, epidermal melanocytes expressing shRNA to TRPML1 did not display increased responses to TRPML3 activators when compared with control cells. This lack of responsiveness could be due to incomplete inhibition of TRPML1 expression, despite the efficacy of the knockdown in heterologous expression situations (Miedel et al., 2008; Samie et al., 2009). An alternative interpretation would be that the influence of TRPML1 on TRPML3 is rather limited because the two proteins may be trafficked differently in native cells. Indeed, endogenous TRPML channels only partially colocalize, and coimmunoprecipitation revealed that only a limited fraction of endogenous TRPML3 interacts with endogenous TRPML1 (Kim et al., 2009; Zeevi et al., 2009). In addition, TRPML3 has been put forward as autoregulator of autophagy (Kim et al., 2009), which could very much limit the occurrence of TRPML3 in the plasma membrane of cells that natively express TRPML3. When we coexpressed dynamin with TRPML3 in HEK293 cells, we indeed found a reduced response to TRPML3 activators. Coexpression of the dominant-negative K44A mutant of dynamin with TRPML3 resulted in small response increases. Although these data are in favor of recent evidence that TRPML3 recycles between the plasma membrane and intracellular compartments, and that autophagy might play a role as a tight regulator of plasma membrane TRPML3, overexpression of the K44A dynamin mutant in human skin melanocytes had no effect on native TRPML3 activator responsiveness.

The sum of differences observed between overexpression studies and expression in primary cells highlight the limitations of cell culture experiments to study trafficking and physiology of TRPML3. Nevertheless, in conclusion, our data show that melanocytes and sensory hair cells do not express activator-responsive TRPML3 in their plasma membrane. Nonresponsiveness could be a result of total absence of the channel protein from the surface of the cells or that TRPML3 exists primarily as a subunit of heteromeric channels in vivo.

SIGNIFICANCE

In this study, we identified 53 compounds that selectively activate TRPML3 with EC_{50} values of <5 μM. The identified activators are surprisingly diverse and can be classified into nine different chemical scaffolds and 19 singletons. The compounds are highly specific for TRPML3, and because they activate the channel with different kinetics and maximal response levels, we content that they comprise an unprecedented collection of tools to investigate activation mechanisms of TRPML3. The observation that combining compound activators with lowering of extracytosolic [Na^+] strongly potentiated the individual responses revealed that at least two different mechanisms cooperatively control TRPML3 activity. They further reveal a wide dynamic range of channel activity, suggesting that TRPML3 response features are stimulus dependent. When we tested the compounds on cells that natively express TRPML3, we uncovered that sensory hair cells failed to respond and that epidermal melanocytes showed only weak or no responses. These results suggest that TRPML3 in native cells is either not present in the plasma membrane or that the protein heteromerizes with other subunits in hair cells and epidermal melanocytes, leading to channels that are not or only weakly responsive to the compounds identified in this screen.

EXPERIMENTAL PROCEDURES

Plasmid Constructs and Cells

All cultured cells were grown and maintained in a standard humidified 37°C incubator, with 5% CO_2. HEK293 and NIH 3T3 cells were maintained in DMEM (Invitrogen), supplemented with 10% fetal bovine serum (Invitrogen), 100 μg/ml penicillin, and 100 μg/ml streptomycin. HEK293 cells stably expressing human TRPML3 and danio rerio TRPN1 (as YFP-fusion proteins) were selected from transfected cells using G418 (geneticin, Sigma-Aldrich) at a final concentration of 0.8 mg/ml and subcloned twice from clearly isolated colonies. Expression vectors were based on pcDNA3.1 (Invitrogen). Mutants were generated from wild-type cDNA templates using QuikChange Site-Directed Mutagenesis Kit (Stratagene) and were verified by sequencing both strands entirely. For calcium imaging and electrophysiological experiments in HEK293 cells, all plasmid constructs were transiently expressed in HEK293 cells with the use of Genejammer (Stratagene) and were measured 24 hr after transfection. In none of the experiments conducted for this study did we observe any anomalous effect of tags on TRPML channel localization and function.

Normal neonatal human epidermal melanocytes (kindly provided by Dr. P. Khavari, Stanford University) were cultured in medium 254 supplemented with HMGS (Cascade Biologic). Using the Amaxa Nucleofector (NHEM-Neo Nucleofector Kit, program U-016), 5×10^5 cells were transfected with 5 μg of plasmid DNA per experiment.

High-Throughput Screen

As part of the Molecular Libraries Probe Production Network (MLPCN; http://mli.nih.gov/mli/) initiative, the high-throughput screening campaign was executed on the automated Kalypsys robotic platform located at the Scripps Research Institute Molecular Screening Center (SRIMSC; Jupiter, FL). Screening results for the TRPML3 (PubChem AID 1448) and TRPN1 (PubChem AID 1424) agonist primary screens, and all subsequent assays within the screening campaign have been deposited into PubChem. Both primary assays were screened against the full MLPCN screening library, which consisted of 217,969 compounds.

The NIH Molecular Libraries Small Molecule Repository (MLSMR, USA) provided compound collections for the primary and initial confirmation assays (dissolved at concentrations up to 10 mM in DMSO). Reference and ordering information for all compounds can be obtained from PubChem website (http://pubchem.ncbi.nlm.nih.gov/) by conducting queries with the PubChem substance identifier (SID). For follow-up studies, compound SF-11 was obtained from Maybridge. Compounds SF-21, SF-31, SF-41, and SN-1 were obtained from Asinex Ltd.. Compounds SF-22 and SF-23 were purchased from Enamine, compounds SF-24, SF-32, and SF-51 were obtained from ChemBridge, and compounds SF-33, SF-61, and SN-2 were obtained from Specs. Compounds SF-71 and SF-81 were purchased from ChemDiv and Key Organics, respectively. All commercially obtained compounds were verified by liquid chromatography-mass spectrometry. Stock solutions of the compounds of 10 mM in DMSO were stored in small aliquots at −80°C.

The assay protocols for both TRPML3 and TRPN1 were identically matched. Cells were diluted in growth medium and dispensed into 1536-well black-wall, clear-bottom plates (Greiner Bio-One) at a concentration of 1500 cells/well, and were allowed to attach for 23 hr at 37°C. Screen Quest Fluo-8 No Wash Calcium mix (ABD Bioquest), prepared according to the manufacturer's instructions, was dispensed into each well. After incubating for 1 hr at 37°C, and 30 min at room temperature, an initial basal fluorescent measurement for 5 s was performed (470–495 nm excitation and 515–575 nm emission) using the $FLIPR^{TETRA}$ fluorescence reader (Molecular Devices). Test compounds (2.99 μM final concentration), DMSO alone (carrier control), or Carbachol (87 μM final concentration, as positive control to elicit calcium influx) was added to sample or appropriate control wells, respectively. Then a real-time

fluorescence measurement was immediately performed for the remaining 120 s of the assay.

The data from each campaign were normalized with basal fluorescence by dividing the maximum fluorescence over the entire real time reading by the initial basal fluorescence. The percentage of activation for each compound was determined using calculated ratios on a per-plate basis as follows: percentage of activation = 100 × (test_compound − low_control) / (high_control − low_control), Where test compound indicates the ratio of fluorescence of wells containing test compound, low control indicates the median average ratio of fluorescence of wells containing DMSO, and high control indicates the median average ratio of fluorescence of wells containing carbachol.

HTS Hit Selection and Activity Cutoff Criteria

To determine agonistic compounds in each primary screen, two values were calculated: (1) the average percentage activation of all compounds tested and (2) three times their standard deviation (Hodder et al., 2003). The sum of these two values was used as a cutoff parameter—that is, any compound that exhibited greater percentage of activation than the cutoff value was considered active. Z' values were determined to monitor assay quality and were calculated as described elsewhere (Zhang et al., 1999). Assay plates were rejected and rerun if Z' was less than 0.5.

Confirmation, Counterscreening, and Dose-Response Assays

Test compounds active in the primary screening campaign were subsequently confirmed using the same assay protocol and hit cutoff value as used in the primary campaign, except that compounds were tested in triplicate. All confirmation and counterscreen assay data has been uploaded to the PubChem website (AID 1526: TRPML3 hit confirmation; AID 1525: TRPN1 counterscreen).

The potency of compounds that passed confirmation and counterscreening was determined using dose-response assays and EC_{50} values were calculated from the resultant data. A 10-point dose-response curve with a 1:3 dilution series from 29.9 μM to 1.5 nM was used, with compounds being tested in triplicate. Compounds exhibiting an EC_{50} value less than 10 μM were considered active. Dose-response assays were also performed against TRPN1 to confirm that compounds identified as TRPML3 agonists were selective (PubChem AID 1562: TRPML3 dose-response determinations; AID 1682: TRPN1 dose-response determinations). Data were analyzed using MDL Assay Explorer (version 3.1, Symyx Solutions). Curve fitting was performed with a four-parameter equation describing a sigmoidal dose-response curve with adjustable baseline. EC_{50} values were generated from fitted curves by solving for the X-intercept at the 50% inhibition level of the Y-intercept.

Calcium Imaging and Electrophysiology

Measurements of $[Ca^{2+}]_i$ with the fluorescent indicators fura-2-AM (Invitrogen) was performed using a monochromator-based imaging system (iMIC platform and Polychrome V monochromator, TILL Photonics). HEK293 cells, plated onto glass coverslips, were loaded with 4 μM fura-2-AM (Invitrogen) in a standard bath solution (SBS) containing 138 mM NaCl, 6 mM KCl, 2 mM $MgCl_2$, 2 mM $CaCl_2$, 10 mM HEPES, and 5.5 mM D-glucose (adjusted to pH 7.4 with NaOH).

Whole-cell currents were recorded with an Alembic Instruments VE-2 amplifier with 100% series resistance compensation, and acquired with JClamp software. The standard bath solution contained 138 mM NaCl, 5.4 mM KCl, 2 mM $MgCl_2$, 2 mM $CaCl_2$, 10 mM HEPES, and 10 mM D-glucose, adjusted to pH 7.4 with NaOH. The standard pipette solution contained 140 mM CsCl, 10 mM HEPES, 3 mM ATP-Na, 1 mM BAPTA, and 2 mM $MgCl_2$, adjusted to pH 7.2. 2-Aminoethyl-diphenyl borate (100 μM) was included in the bath solution to block gap junctions and had no effect on the expressed channels. Unless indicated differently, the plots shown were responses to 10 ms voltage steps (holding potential, +10 mV) between −200 mV and +100 mV in 20 mV incremental steps, normalized by cell capacitance (pF).

RNA Interference (RNAi)

Specific and efficient RNAi-mediated knock down of endogenous human TRPML1 expression has been recently reported (Miedel et al., 2008; Samie et al., 2009). Oligonucleotide 5′-GCTACCTGACCTTCTTCCACA-3′ (Samie et al., 2009) was cloned into the shRNA expression vector U6 RNA Pol III (Invitrogen). HEK293 cells were cotransfected with 3 μg of shRNA to human TRPML1 and 1 μg human TRPML1-YFP plasmid using Genejammer, as described above. A mutant isoform of TRPML1-YFP (C1218T, silent mutation) was cotransfected with TRPML1 shRNA as a control to determine efficacy (Figure S5A). Human epidermal melanocytes were cotransfected with 5 μg TRPML1 shRNA and 2 μg pcDNA3.1-YFP using Amaxa Nucleofector technology as described above.

Biotinylation, Western Blots, and Immunocytochemistry

Transfected HEK293 cells were analyzed 15–16 hr after transfection, washed, and surface biotinylated with Sulfo-NHS-LC-LC-biotin solution (Pierce), as described elsewhere (Grimm et al., 2007). All samples were then processed for western blot analysis as described elsewhere (Cuajungco et al., 2006), and visualized using an anti-GFP monoclonal antibody (JL-8; Clontech). Detection was performed with IRDye 700- and IRDye 800-conjugated secondary antibodies (Rockland Immunochemicals, Gilbertsville, PA) and scanning with the Odyssey infrared imaging system (LI-COR Biosciences, Lincoln, NE). Signal quantification was conducted with Image J software (http://rsb.info.nih.gov/ij/). Immunocytochemistry with mouse monoclonal pan-Cadherin CH-19 (Abcam, 1:500) and TRITC-conjugated goat anti mouse IgG1 (Jackson ImmunoResearch), was performed as described elsewhere (Cuajungco et al., 2006).

ACCESSION NUMBERS

Screening results for the primary and confirmation screens have been deposited in the PubChem BioAssay database with accession codes AID 1424, 1448, 1525, 1526, 1538, 1562, 1660, 1682, and 1809.

SUPPLEMENTAL INFORMATION

Supplemental Information includes two tables and six figures and can be found with this article online at doi:10.1016/j.chembiol.2009.12.016.

ACKNOWLEDGMENTS

We thank Teresa Nicolson (OHSU) for providing the TRPN1 cDNA, and Shmuel Muallem, Hyun-Jin Kim, and Joseph Albanesi (UT Southwestern) for providing dynamin wild-type and dynamin K44A mutant cDNAs. We also thank Lars Becker for critically reading the manuscript; Michael Schnee and Anthony Ricci for expert advice in patch-clamp techniques; Shiying Tao and Paul Khavari for providing purified human skin melanocyte cultures; Pierre Baillargeon and Lina DeLuca (Scripps Research Institute Molecular Screening Center) for their assistance with compound management; and Louis Scampavia (Scripps, Florida) for LC-MS analysis of the presented compounds. This work was supported by the National Institutes of Health (grants MH083077, DC004563, and P30 DC010363 to S.H. and grant U54MH084512 to P.H.).

Received: October 10, 2009
Revised: December 22, 2009
Accepted: December 31, 2009
Published: February 25, 2010

REFERENCES

Atiba-Davies, M., and Noben-Trauth, K. (2007). TRPML3 and hearing loss in the varitint-waddler mouse. Biochim. Biophys. Acta *1772*, 1028–1031.

Bargal, R., Avidan, N., Ben-Asher, E., Olender, Z., Zeigler, M., Frumkin, A., Raas-Rothschild, A., Glusman, G., Lancet, D., and Bach, G. (2000). Identification of the gene causing mucolipidosis type IV. Nat. Genet. *26*, 118–123.

Cuajungco, M.P., Grimm, C., Oshima, K., D'Hoedt, D., Nilius, B., Mensenkamp, A.R., Bindels, R.J., Plomann, M., and Heller, S. (2006). PACSINs bind to the TRPV4 cation channel. PACSIN 3 modulates the subcellular localization of TRPV4. J. Biol. Chem. *281*, 18753–18762.

Di Palma, F., Belyantseva, I.A., Kim, H.J., Vogt, T.F., Kachar, B., and Noben-Trauth, K. (2002). Mutations in Mcoln3 associated with deafness and

pigmentation defects in varitint-waddler (Va) mice. Proc. Natl. Acad. Sci. USA *99*, 14994–14999.

Grimm, C., Cuajungco, M.P., van Aken, A.F., Schnee, M., Jörs, S., Kros, C.J., Ricci, A.J., and Heller, S. (2007). A helix-breaking mutation in TRPML3 leads to constitutive activity underlying deafness in the varitint-waddler mouse. Proc. Natl. Acad. Sci. USA *104*, 19583–19588.

Grimm, C., Jörs, S., and Heller, S. (2009). Life and death of sensory hair cells expressing constitutively active TRPML3. J. Biol. Chem. *284*, 13823–13831.

Hodder, P., Cassaday, J., Peltier, R., Berry, K., Inglese, J., Feuston, B., Culberson, C., Bleicher, L., Cosford, N.D., Bayly, C., et al. (2003). Identification of metabotropic glutamate receptor antagonists using an automated high-throughput screening system. Anal. Biochem. *313*, 246–254.

Hofmann, T., Schaefer, M., Schultz, G., and Gudermann, T. (2002). Subunit composition of mammalian transient receptor potential channels in living cells. Proc. Natl. Acad. Sci. USA *99*, 7461–7466.

Kim, H.J., Li, Q., Tjon-Kon-Sang, S., So, I., Kiselyov, K., and Muallem, S. (2007). Gain-of-function mutation in TRPML3 causes the mouse Varitint-Waddler phenotype. J. Biol. Chem. *282*, 36138–36142.

Kim, H.J., Li, Q., Tjon-Kon-Sang, S., So, I., Kiselyov, K., Soyombo, A.A., and Muallem, S. (2008). A novel mode of TRPML3 regulation by extracytosolic pH absent in the varitint-waddler phenotype. EMBO J. *27*, 1197–1205.

Kim, H.J., Soyombo, A.A., Tjon-Kon-Sang, S., So, I., and Muallem, S. (2009). The Ca(2+) channel TRPML3 regulates membrane trafficking and autophagy. Traffic *10*, 1157–1167.

Miedel, M.T., Weixel, K.M., Bruns, J.R., Traub, L.M., and Weisz, O.A. (2006). Posttranslational cleavage and adaptor protein complex-dependent trafficking of mucolipin-1. J. Biol. Chem. *281*, 12751–12759.

Miedel, M.T., Rbaibi, Y., Guerriero, C.J., Colletti, G., Weixel, K.M., Weisz, O.A., and Kiselyov, K. (2008). Membrane traffic and turnover in TRP-ML1-deficient cells: a revised model for mucolipidosis type IV pathogenesis. J. Exp. Med. *205*, 1477–1490.

Nagata, K., Zheng, L., Madathany, T., Castiglioni, A.J., Bartles, J.R., and Garcia-Anoveros, J. (2008). The varitint-waddler (Va) deafness mutation in TRPML3 generates constitutive, inward rectifying currents and causes cell degeneration. Proc. Natl. Acad. Sci. USA *105*, 353–358.

Patapoutian, A., Tate, S., and Woolf, C.J. (2009). Transient receptor potential channels: targeting pain at the source. Nat. Rev. Drug Discov. *8*, 55–68.

Ramsey, I.S., Delling, M., and Clapham, D.E. (2006). An introduction to TRP channels. Annu. Rev. Physiol. *68*, 619–647.

Samie, M.A., Grimm, C., Evans, J.A., Curcio-Morelli, C., Heller, S., Slaugenhaupt, S.A., and Cuajungco, M.P. (2009). The tissue-specific expression of TRPML2 (MCOLN-2) gene is influenced by the presence of TRPML1. Pflugers. Arch. *459*, 79–97.

Simmons, D.D., Mansdorf, N.B., and Kim, J.H. (1996). Olivocochlear innervation of inner and outer hair cells during postnatal maturation: evidence for a waiting period. J. Comp. Neurol. *370*, 551–562.

van Aken, A.F., Atiba-Davies, M., Marcotti, W., Goodyear, R.J., Bryant, J.E., Richardson, G.P., Noben-Trauth, K., and Kros, C.J. (2008). TRPML3 mutations cause impaired mechano-electrical transduction and depolarization by an inward-rectifier cation current in auditory hair cells of varitint-waddler mice. J. Physiol. *586*, 5403–5418.

Venkatachalam, K., Hofmann, T., and Montell, C. (2006). Lysosomal localization of TRPML3 depends on TRPML2 and the mucolipidosis-associated protein TRPML1. J. Biol. Chem. *281*, 17517–17527.

Vergarajauregui, S., and Puertollano, R. (2006). Two di-leucine motifs regulate trafficking of mucolipin-1 to lysosomes. Traffic *7*, 337–353.

Waguespack, J., Salles, F.T., Kachar, B., and Ricci, A.J. (2007). Stepwise morphological and functional maturation of mechanotransduction in rat outer hair cells. J. Neurosci. *27*, 13890–13902.

Xu, H., Delling, M., Li, L., Dong, X., and Clapham, D.E. (2007). Activating mutation in a mucolipin transient receptor potential channel leads to melanocyte loss in varitint-waddler mice. Proc. Natl. Acad. Sci. USA *104*, 18321–18326.

Yamasaki, M., Komune, S., Shimozono, M., Matsuda, K., and Haruta, A. (2000). Development of monovalent ions in the endolymph in mouse cochlea. ORL J. Otorhinolaryngol. Relat. Spec. *62*, 241–246.

Zeevi, D.A., Frumkin, A., and Bach, G. (2007). TRPML and lysosomal function. Biochim. Biophys. Acta *1772*, 851–858.

Zeevi, D.A., Frumkin, A., Offen-Glasner, V., Kogot-Levin, A., and Bach, G. (2009). A potentially dynamic lysosomal role for the endogenous TRPML proteins. J. Pathol. *219*, 153–162.

Zhang, J.H., Chung, T.D., and Oldenburg, K.R. (1999). A simple statistical parameter for use in evaluation and validation of high throughput screening assays. J. Biomol. Screen. *4*, 67–73.